J Mater Sci (2006) 41:5292–5301
DOI 10.1007/s10853-006-0263-9

The effect of Copper alloying additions on the crystallization of an amorphous Fe–Si–B alloy

Y. R. Zhang · R. V. Ramanujan

Received: 13 March 2005 / Accepted: 17 October 2005 / Published online: 6 June 2006

Abstract The effect of Cu alloying additions on the crystallization of Fe–Si–B alloy was studied. The selected alloys compositions are $Fe_{77.5}Si_{13.5}B_9$ and $Fe_{76.5}Si_{13.5}B_9Cu_1$. By comparing their crystallization temperatures, activation energy of crystallization, phase formation and microstructural evolution after heat treatment, the effect of Cu alloying additions was determined. It was found that Cu alloying additions reduced the crystallization temperature as well as the activation energy of the crystallization. Although the phases formed in both alloys were Fe_3Si and Fe_3B phases the microstructures were dramatically different: a dendritic microstructure was observed in the case of the Fe–Si–B alloy, while spheriodal crystals around 100 nm in size were observed in the case of the Fe–Si–B–Cu alloy. Cu alloying addition increased the saturation magnetization during primary crystallization whereas it decreased the saturation magnetization after secondary crystallization began. Interestingly, for both alloys the same trends of the magnetization and coercivity measurements were observed except that the extent of the changes were higher in the case of the Fe–Si–B–Cu alloy than that of the Fe–Si–B alloy.

Introduction

The Fe–Si–B–Cu–Nb amorphous alloy with the compositions: $Fe_{73.5}Si_{13.5}B_9Nb_3Cu_1$ after appropriate annealing exhibits excellent magnetic properties, these superior properties result from crystallization of an initially amorphous material, leading to the formation of nanocrystals (about 10 nm in size) of the Fe_3Si phase in the remaining amorphous matrix [1]. These nanocrystals resulted in a reduction of the coercivity as a result of the averaging magnetic anisotropy leading to good soft magnetic properties, as suggested by Herzer [2]. This alloy is now available commercially as Finemet. Concerning the role of copper in this kind of alloy, there have been many earlier reports, the most prominent studies have been conducted by Hono and Ayers [3–7]. These studies were conducted in the alloy with both Cu and Nb alloying additions. It is well known that containing Cu and Nb elements will influence the thermodynamics and kinetics of the crystallization in the Finemet alloy. In the case of combined additions, copper has been reported to increase the nucleation density of the crystals formed by primary crystallization. However, in order to obtain fundamental understanding of the effects of Cu and Nb alloying additions in the Finemet alloy particular attention should be paid to separate rather than combined additions of Cu and Nb to the reference Fe–Si–B alloy. Hence the $Fe_{76.5}Si_{13.5}B_9Cu_1$ alloy was selected and compared to the $Fe_{77.5}Si_{13.5}B_9$ alloy. For the $Fe_{76.5}Si_{13.5}B_9Cu_1$ alloy earlier work on its crystallization process has provided information concerning thermal properties, phase formation and microstructure observations [8–14]. However, a study combining these aspects has not been reported and this is the object of the present work. In addition, this study can provide a reference for the understanding of the effect of the Cu alloying addition in the Finemet alloy containing both Cu and Nb.

This paper describes the effect of Cu alloying additions in a Fe–Si–B alloy by comparing the thermal behavior, phase formation, microstructural observations and

Y. R. Zhang · R. V. Ramanujan (✉)
School of Materials Science and Engineering, Nanyang Technological University, Nanyang Avenue, Singapore 639798, Singapore
e-mail: ramanujan@ntu.edu.sg

magnetic properties of a Fe–Si–B–Cu alloy with those of a Fe–Si–B alloy. The two alloy compositions ($Fe_{77.5}Si_{13.5}B_9$ and $Fe_{76.5}Si_{13.5}B_9Cu_1$) were selected based on the composition of the Finemet alloy ($Fe_{73.5}Si_{13.5}B_9Nb_3Cu_1$). Characterization was performed using the differential scanning calorimetry (DSC), X-ray diffraction (XRD), transmission electron microscope (TEM), and vibrating sample magnetometer (VSM).

Experimental procedure

Two alloy compositions were examined: $Fe_{77.5}Si_{13.5}B_9$ and $Fe_{76.5}Si_{13.5}B_9Cu_1$. One atomic percent of Cu element was chosen based on the concentration of Cu element added in Finemet alloys. The material used is 20 μm thick and 25 mm wide ribbon, both alloys are amorphous as received as shown by the XRD measurements. A NETZSCH DSC-404C was employed to study the thermal behavior. A RIGAKU DMAX 2200 was used for X-ray diffraction studies. Heat treatment conditions were selected according to the DSC results and heat treatment conditions of 420, 490, 515, 550, 600 and 640 °C for 1 h were employed. Heat treatment was carried out in the vacuum furnace (10^{-5}torr). A JEOL 2010 Transmission Electron Microscope (TEM) with an accelerating voltage of 200 kV was employed. The samples prepared for TEM observation were cut into 3 mm discs before heat-treatment and subsequently ion-milled. The measurement of the saturation magnetization of the materials (at B = 1.3 T) was made by a LakeShore vibrating sample magnetometer. All the measurements were conducted three times to minimize errors.

Results

By means of DSC the crystallization temperatures of the selected alloys were measured at heating rates of 2, 5, 10, and 20 K/min, as shown in Fig. 1a and b. Figure 1a and b show the DSC curves for the Fe–Si–B and Fe–Si–B–Cu alloys, respectively obtained for the heating rates of 2, 5, 10 and 20 K/min. Two exothermic peaks were observed for both alloys. The crystallization temperatures at a heating rate of 10 K/min for the first peak in the case of the Fe–Si–B alloy is at 526.6 °C while in the case of the Fe–Si–B–Cu alloy it occurs at 466.4 °C, which is consistent with earlier reports [10–15]. At the same time the Cu alloying addition increased the gap between the first peak and second peak (Fig. 1b). The crystallization temperatures and exothermic enthalpies for both alloys are provided in Table 1a and b.

By using the Doyle–Ozawa Method the activation energies of different alloys can be calculated by means of the following equation [16]:

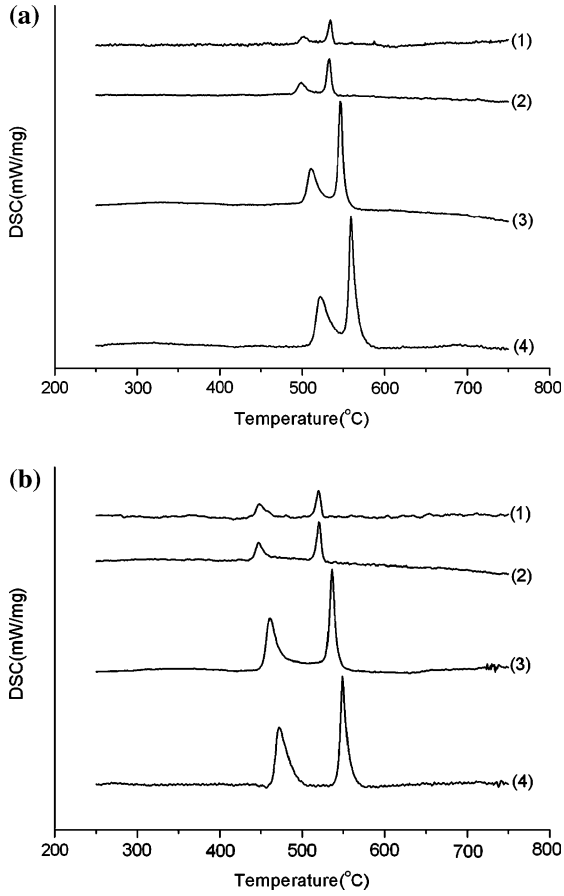

Fig. 1 (**a**) DSC results for the Fe–Si–B alloy at heating rates of (1) 2 K/min, (2) 5 K/min, (3) 10 K/min and (4) 20 K/min; (**b**) DSC results for the Fe–Si–B–Cu alloy at heating rates of (1) 2 K/min, (2) 5 K/min, (3) 10 K/min and (4) 20 K/min

$$\mathrm{Log}b = \mathrm{Log}[AE/RF(\alpha)] - 2.315 - 0.4567E/(RT)$$

where b is the heating rate, A is a constant, $F(\alpha)$ is the crystallized fraction, T is the temperature corresponding to the crystallized fraction, E is the activation energy, R is gas constant: 8.314 J/K.

Plotting Log$b$ as the Y-axis and $1/T$ as the X-axis a straight line can be obtained, the slope of which is $-0.4567E/R$, thus the activation energy can be calculated (Fig. 2a–d), the results are tabulated in Table 2. The activation energy for the first crystallization temperature in the case of the Fe–Si–B alloy is 535.8 kJ/mol while that for the Cu-containing alloy is 259.7 kJ/mol which showed that Cu alloying addition made primary crystallization easier suggesting that it enhances the kinetics of crystallization [17].

The received alloys were identified by XRD and broad peaks were observed, indicating the amorphous alloy (Fig. 3). Both alloys were heat treated at various temperatures for 1 h: 420, 490, 500, 515, 550, 600 and 640 °C. The phases formed in the Fe–Si–B alloy was studied by

Table 1 The temperatures corresponding to exothermic effects for the (a) Fe–Si–B alloy and (b) Fe–Si–B–Cu alloy

Heating rate (K/min)		2	5	10	20
Panel (a)					
1st peak	T_{x1} (°C)	496.4	510.9	518.1	522.8
	T_{p1} (°C)	511.7	518.9	526.6	532.1
	T_{e1} (°C)	503.4	529.7	538.4	547
	ΔH (J/g)	24.7	31.3	37.6	46.7
2nd peak	T_{x2} (°C)	529.4	537.6	546.9	—
	T_{p2} (°C)	534.2	542.7	551.8	567.8
	T_{e2} (°C)	537.5	547.1	557.4	576.5
	ΔH (J/g)	50.3	59.5	64.9	69.6
Panel (b)					
1st peak	T_{x1} (°C)	440.1	449.0	457.7	474.1
	T_{p1} (°C)	449	456.9	466.4	482.1
	T_{e1} (°C)	459.8	466.4	477.6	498.6
	ΔH (J/g)	34.7	37.0	39.5	47.5
2nd peak	T_{x2} (°C)	515.5	514.4	524.6	543.8
	T_{p2} (°C)	519.7	520.4	530.5	548.9
	T_{e2} (°C)	523.4	525.3	536.6	556.8
	ΔH (J/g)	42	43.3	44.6	46.1

T_x the onset temperature of the crystallization, T_p the peak temperature of the crystallization, T_e the ending temperature of the crystallization, ΔH the enthalpy of the whole crystallization process

XRD (Fig. 4), the results indicated that the Fe_3Si phase was the dominant phase as the annealing temperature increased from 490 °C to 640 °C. In the case of the Fe–Si–B alloy the Fe_3B phase was observed, which indicated the initiation of secondary crystallization formed at 515 °C. On the other hand with Cu alloying additions primary crystallization

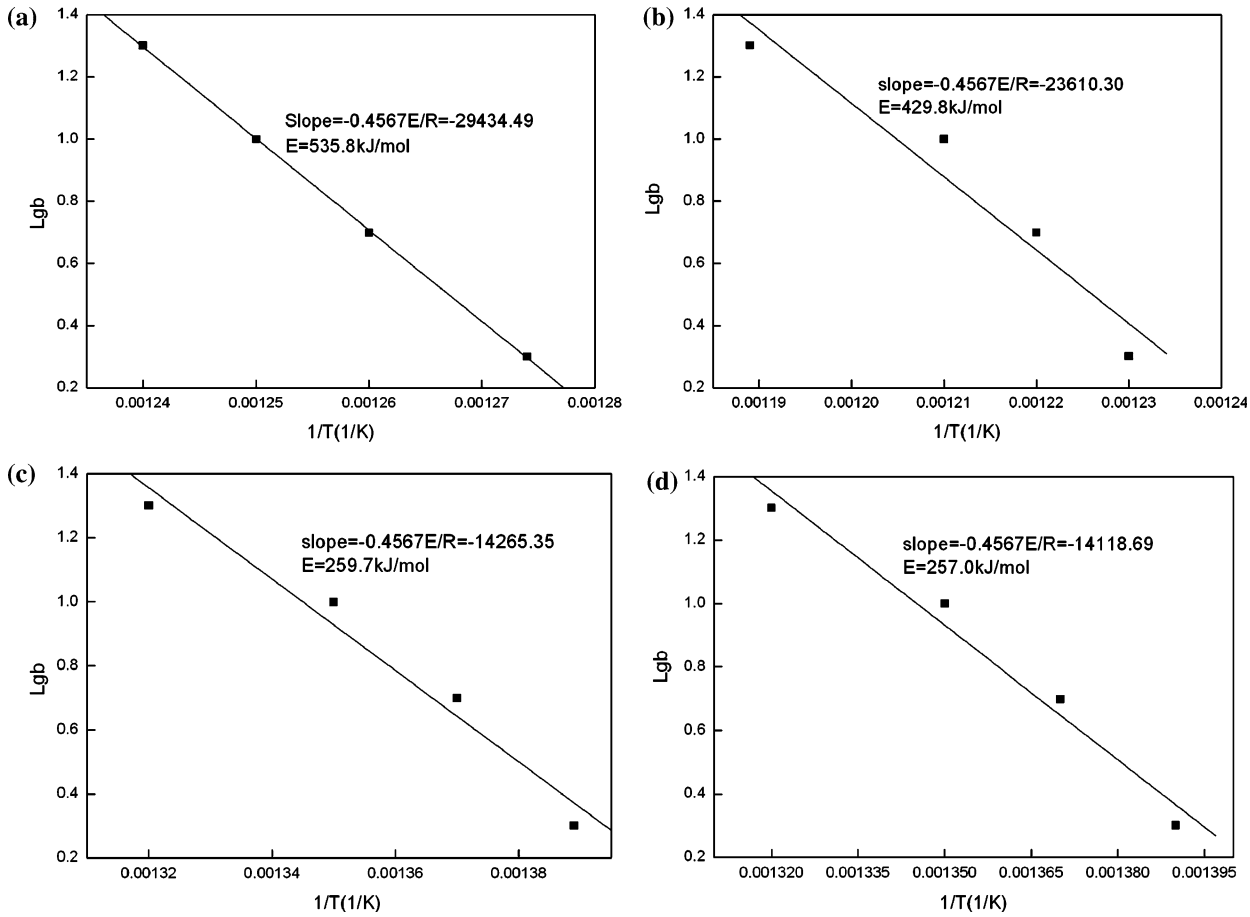

Fig. 2 Activation energy obtained from DSC measurement for the first peak and second crystallization peak: (**a**) and (**b**) for $Fe_{77.5}Si_{13.5}B_9$ alloy, (**c**) and (**d**) for $Fe_{76.5}Si_{13.5}B_9Cu_1$ alloy, respectively

Table 2 Calculated activation energy of different alloys

	$Fe_{76.5}Cu_1Si_{13.5}B_9$				$Fe_{77.5}Si_{13.5}B_9$			
Heating rate (K/min)	2	5	10	20	2	5	10	20
First peak (°C)	449	456.9	466.4	482.1	511.7	518.9	526.6	532.1
Activation energy (kJ/mol)	259.7 ± 32.24				535.8 ± 5.86			
Heating rate (K/min)	2	5	10	20	2	5	10	20
Second peak (°C)	519.7	520.4	530.5	548.9	534.2	542.7	551.8	567.8
Activation energy (kJ/mol)	257 ± 29.89				429.8 ± 38.70			

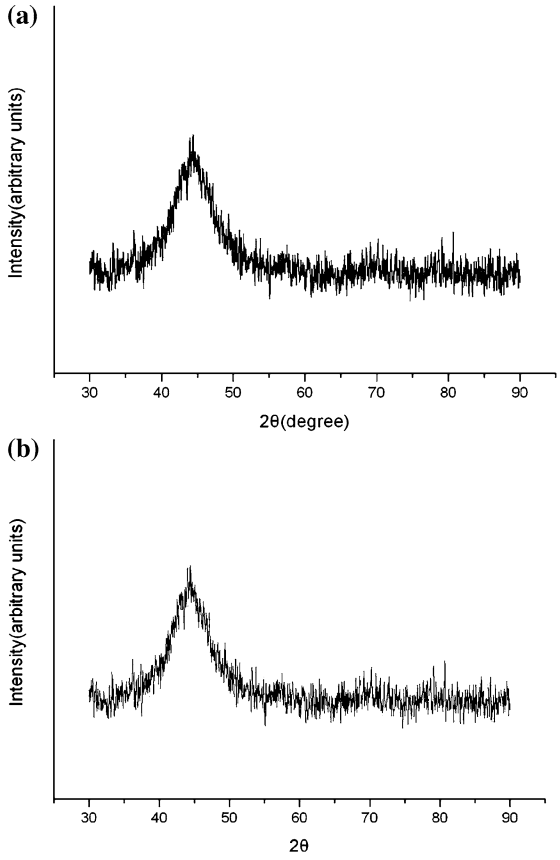

Fig. 3 XRD results of the received amorphous alloys: (**a**) $Fe_{77.5}Si_{13.5}B_9$ alloy (**b**) $Fe_{76.5}Si_{13.5}B_9Cu_1$ alloy

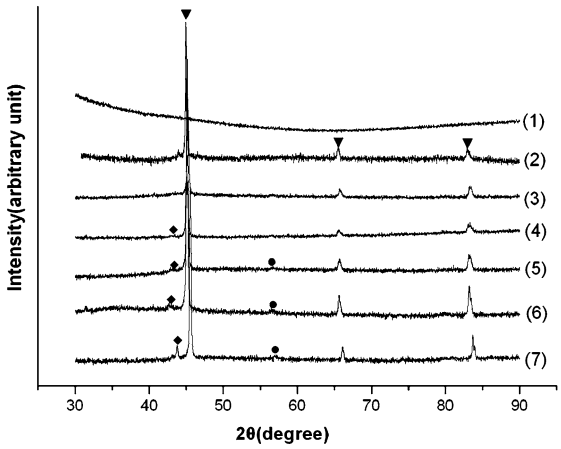

Fig. 4 XRD results for the Fe–Si–B alloy heat treated at different temperature for 1 h: (1) 420 °C, (2) 490 °C, (3) 500 °C, (4) 515 °C, (5) 550 °C, (6) 600 °C, and (7) 640 °C: Fe_3Si (▼), Fe_3B (♦), Fe_2B (●)

occurred at lower temperatures, the Fe_3Si phase was identified at 420 °C (Fig. 5) and the Fe_3B phase formed at 500 °C. This showed that both the primary and secondary crystallization temperatures in the case of the Fe–Si–B–Cu alloy are lower than those of the Fe–Si–B alloy, which is consistent with the DSC results.

Transmission electron microscopy studies could be used to obtain more information about the microstructural evolution for the selected alloys. The halo rings were observed in the SADP of the received amorphous alloys (Fig. 6). For the Fe–Si–B alloy the morphology of the first crystallization products at 490 °C for 1 h is dendritic, the branches are composed of closely spaced precipitates as shown by the arrow in Fig. 7. For the Fe–Si–B–Cu alloy the microstructural evolution was significantly different: for a heat treatment temperature of 420 °C, instead of a dendritic morphology, spheroidal crystals less than 100 nm in size were observed as the first crystallization products (Fig. 8a). Figure 8b shows a higher magnification micrograph of spheriodal crystals about 50 nm in size, the corresponding SADP as shown in Fig. 8c was indexed as the bcc Fe_3Si phase which is consistent with the XRD identification in Fig. 5. At higher temperatures of 490 °C, more crystals precipitated from the amorphous matrix and those originally formed spheriodal crystals grew larger to more than 100 nm in size (Fig. 8d). At 500 °C, secondary crystallization occurred with the formation of a striped structure of the Fe_3B phase, as indicated by the arrow in Fig. 8e.

In order to obtain a better understanding of the striped microstructure of the Fe_3B phase the BF and corresponding DF micrographs are provided in Fig. 9. These striped products formed from the remaining amorphous matrix between the spheroidal Fe_3Si crystals. At the same time, the Fe_3Si phase formed from the amorphous matrix during the secondary crystallization was in the form of crystals larger than 200 nm, the crystal structure was found by SADP analysis to possess the DO_3 ordered structure (Fig. 10).

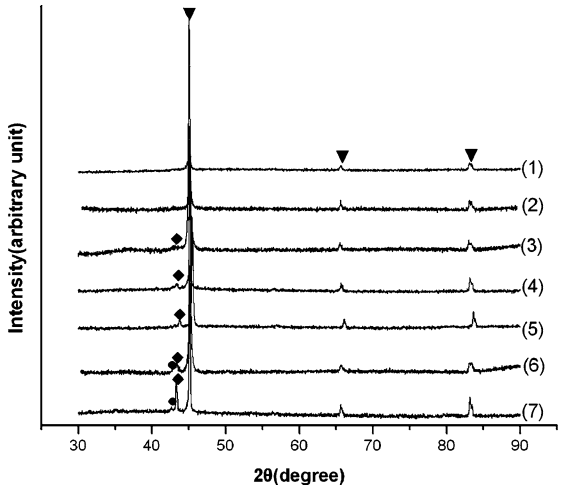

Fig. 5 XRD results for Fe–Si–B–Cu alloy heat treated at different temperatures for 1 h: (1) 420 °C, (2) 490 °C, (3) 500 °C, (4) 515 °C, (5) 550 °C, (6) 600 °C, and (7) 640 °C: Fe_3Si (▼), Fe_3B (♦), Fe_2B (●)

Magnetic properties such as coercivity and saturation magnetization were measured by VSM. The results are shown in Figs. 11 and 12. Compared with the Fe–Si–B alloy the saturation magnetization was less while the coercivity was greater in the Fe–Si–B–Cu alloy. For the as-received amorphous alloys the saturation magnetization is 1.3 T and the coercivity is 60 A/m as indicated in Figs. 11 and 12. After crystallization began, the saturation magnetization decreased while the coercivity of both alloys increased due to structural relaxation. The magnetic properties of both alloys showed similar changing trends as the annealing temperature was increased. As the annealing temperature was increased from 420 °C to 490 °C the magnetization increased significantly from 1.2 T to 1.6 T while the coercivity remained almost the same. After both alloys were heat treated at 500 °C for 1 h saturation magnetization decreased and the coercivity increased sharply from 1 kA/m to about 4 kA/m.

Discussion

Thermal properties

The DSC curves of both the Fe–Si–B alloy and the Fe–Si–B–Cu alloy exhibit two exothermic peaks which means that there exists a two-step crystallization processes before the final stable phases are obtained. The first peak corresponds to the formation of the Fe_3Si phase and the second peak indicates the appearance of the Fe_3B compound. This analysis can be verified by the XRD data in Figs. 4 and 5, respectively. The two peaks of Fe–Si–B alloy are close to each other, compared with one of the alloy with Cu additions. It was also observed in the DSC data that there was a significant lowering in the value of the first crystallization temperature from 511 °C to 449 °C when 1 at% Cu was added to Fe–Si–B alloy which indicated crystallization began at lower temperature, this is because Cu destabilized the amorphous Fe–Si–B phase, as was reported earlier [15]. The addition of Cu decreased the primary crystallization temperature by more than 60 °C, much more than that of the secondary crystallization temperature, indicating that Cu alloying additions changed the kinetics and thermodynamics of the first crystallization processes more significantly than those of the second crystallization processes. In addition, the calculated activation energy also supported this assumption, Cu alloying

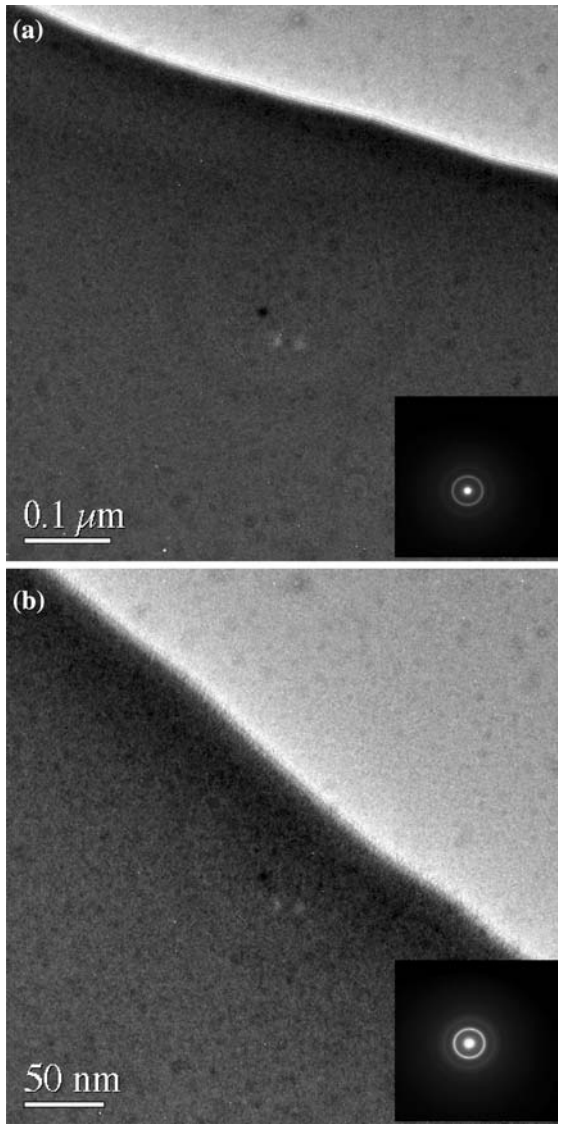

Fig. 6 TEM micrograph and SADP of the received amorphous alloys: (**a**) $Fe_{77.5}Si_{13.5}B_9$ alloy and (**b**) $Fe_{76.5}Si_{13.5}B_9Cu_1$ alloy

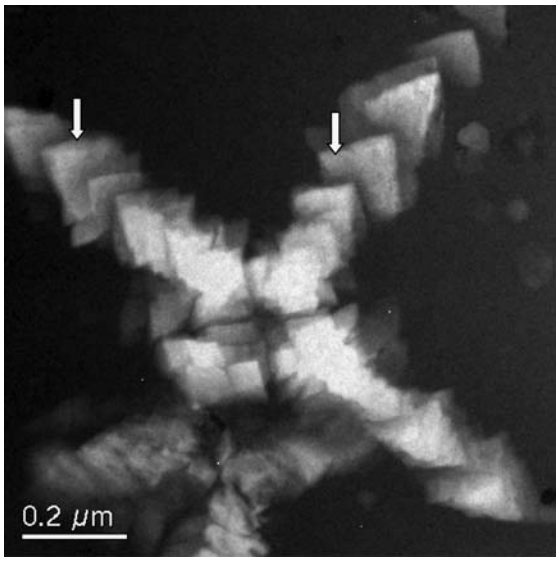

Fig. 7 BF TEM Micrograph of Fe–Si–B alloy heat treatment at 490 °C for 1 h

additions reduced the activation energy of the first crystallization from 376 kJ/mol in the case of the Fe–Si–B alloy to 236 kJ/mol in the case of the Fe–Si–B–Cu alloy, while for the activation energy of secondary crystallization a reduction of 73 kJ/mol was observed with Cu alloying addition.

Crystallization process

In the case of the Fe–Si–B alloy, from the XRD results, it was observed that primary crystallization did not occur for a heat treatment time of 1 h until 490 °C while for the Fe–Si–B–Cu alloy primary crystallization occurred at 420 °C for 1 h. This is consistent with the DSC results that Cu alloying addition reduced the primary crystallization temperature and made crystallization earlier. Although the phases formed after primary crystallization are the same, i.e. the Fe_3Si phase, the morphologies differed considerably, however only 1 at% Cu drastically changes the morphology of the Fe_3Si phase [18]. In the case of the Fe–Si–B alloy the morphology of the primary crystallization product is an anisotropic dendrite with branches composed of closely spaced individual precipitates, while in the case of the Fe–Si–B–Cu alloy, instead of a dendritic morphology, much more isotropic spheroidal precipitates were observed. From Fig. 7b it was observed that this sphreriodal precipitate is about 50 nm in size, this finding differs from Efthimiadis' report that the first crystallization products of the $Fe_{75-x}Cu_xSi_9B_{16}$ ($x < 4$) alloys are dendrites [18]. This spheriodal crystal was found by SADP analysis to be bcc Fe_3Si phase, consistent with XRD results (Fig. 5).

In the Fe–Si–B alloy systems, a dendritic morphology is commonly observed due to solute rejection during crystallization resulting in constitutional supercooling. The condition for no constitutional supercooling is that [19]:

$$(T_1'/v) > \frac{(T_1 - T_3)}{D} \tag{1}$$

where T_1' stands for the temperature gradient at the interface between the matrix and the precipitate as the crystallization began; T_1–T_3 is the temperature difference between the matrix and the precipitate after crystallization is completed; D is the diffusivity in the matrix; and v is the growth rate.

From the equation above constitutional supercooling can be avoided by reduced v (growth rate) or increased D (the diffusivity in the matrix). It has been reported earlier that with Cu alloying additions, the primary crystallization growth rate will be reduced. The nucleation rate will be increased due to additional nuclei provided by Cu alloying addition perhaps by reducing the activation energy for nucleation [9, 20, 21]. As found in the experimental alloy, the growth rate, v, will be decreased by Cu alloying addition which is helpful to avoid constitutional supercooling. Concerning the effect on diffusivity in the matrix (D) by Cu alloying addition, with Cu alloying addition the crystallization began at lower temperature and the diffusivity in the matrix will be less at lower crystallization temperature. On the other hand, a higher density of nuclei induced by Cu alloying addition will produce more solute rejection in the matrix during crystallization which will increase the concentration in the matrix, thus increasing the diffusivity. Thus the effect of Cu alloying addition on the diffusivity in the matrix (D) is a compromise between these effects. Hence, it is suggested that the constitutional supercooling will be avoided by Cu alloying addition mainly by a reduction of the growth rate and by a more isotropic interfacial energy between the matrix and the crystal. Thus instead of dendritic morphology, a spheriodal morphology was observed in the Fe–Si–B–Cu alloy.

As the annealing temperature of the crystallization of the Fe–Si–B–Cu alloy was increased to 490 °C, more spheriodal crystals formed from the amorphous matrix and the volume fraction of such crystals increased. When the annealing temperature was increased to 500 °C, secondary crystallization was observed corresponding to the formation of the Fe_3B phase (Fig. 4). This phase formed along the spheriodal crystal boundary in the form of a striped morphology (as shown by the arrows in Figs. 8, 9). This morphology has not been previously reported [18]. As the Fe_3Si spheriodal crystals formed, boron was rejected into the matrix which is helpful for the formation of the Fe_3B phase.

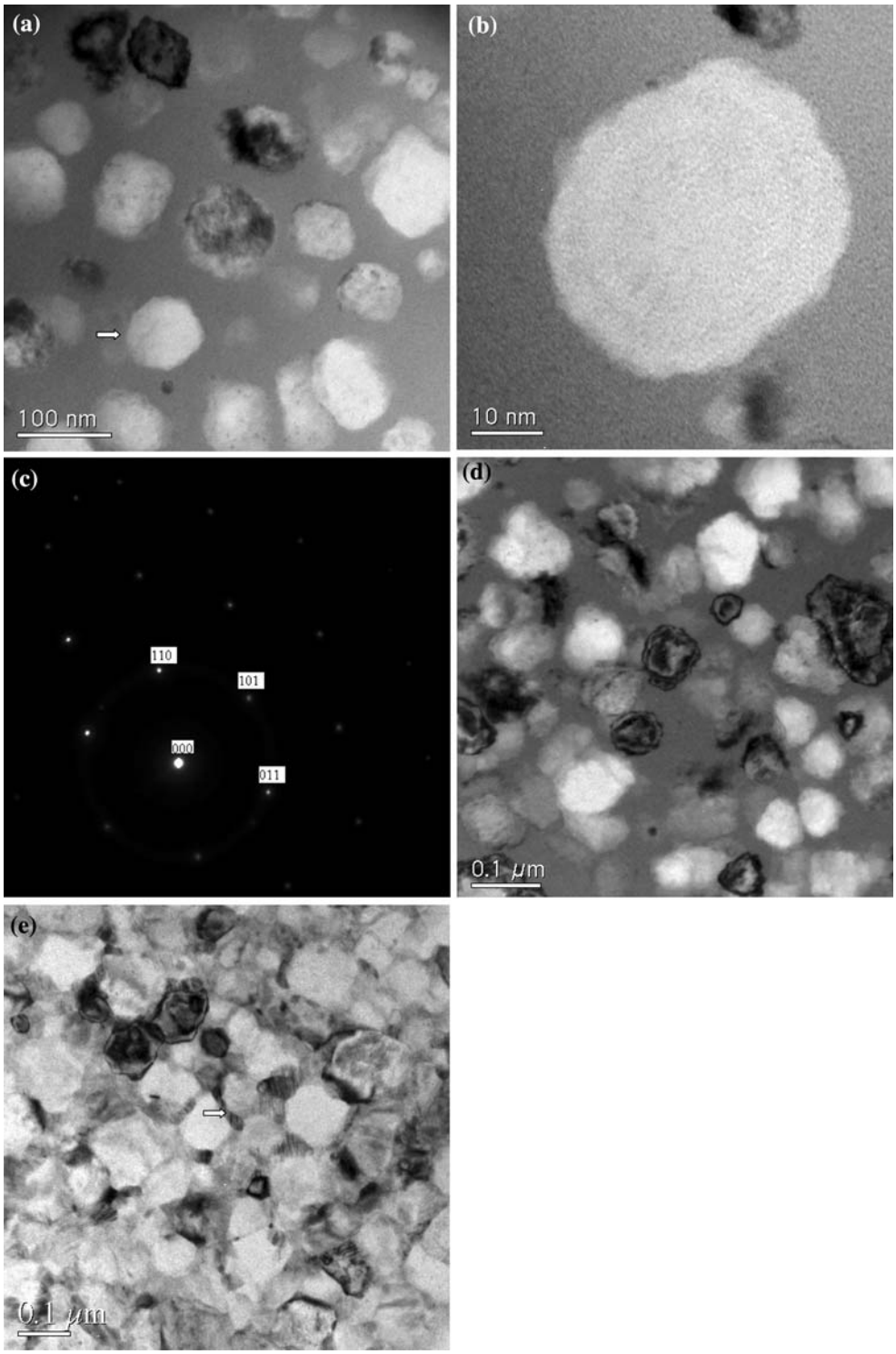

Fig. 8 (**a**) BF TEM Micrograph of Fe–Si–B–Cu alloy heat treatment at 420 °C for 1 h. (**b**) BF TEM Micrograph and (**c**) SADP of the precipitate indicated by arrow in Fig 8(a): zone axis: [$1\bar{1}1$]. (**d**) Bright field micrograph of Fe–Si–B–Cu alloy heat treatment at 490°C for 1 h; (**e**) Bright field micrograph of the Fe–Si–B–Cu alloy heat treatment at 640°C for 1 h

The phases formed after crystallization is complete in the case of the Fe–Si–B–Cu alloy are the Fe_3Si, Fe_2B and Fe_3B phases. The final product of crystallization was mainly spheriodal crystals of Fe_3Si phase around 100 nm in size. Along the crystal boundary the Fe_3B and Fe_2B phases with striped morphology were observed. The Fe_3Si phase formed as large crystals about 200 nm in size (Fig. 10) during secondary crystallization, the crystal structure has an ordered DO_3 structure, which has not been reported in previous investigations [6, 7, 18].

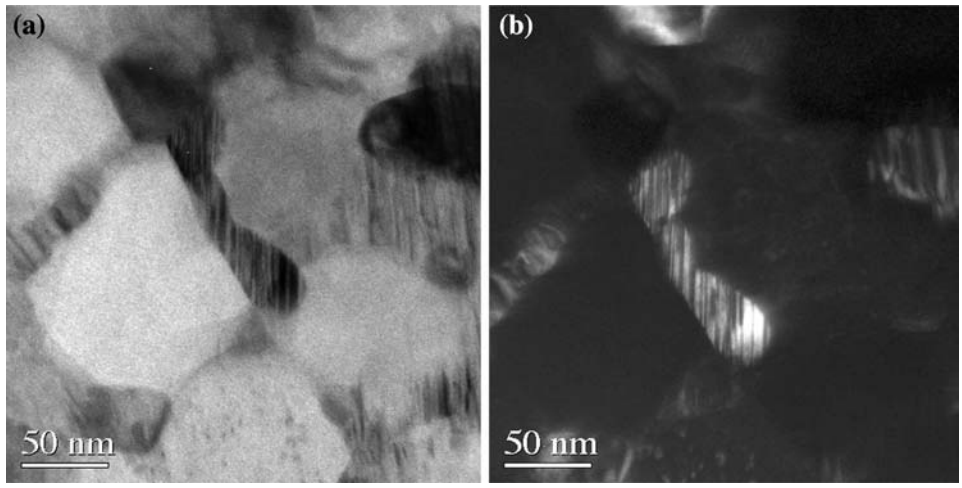

Fig. 9 BF (**a**) and DF (**b**) TEM micrographs of the striped morphology indicated by arrow in Fig 8(c)

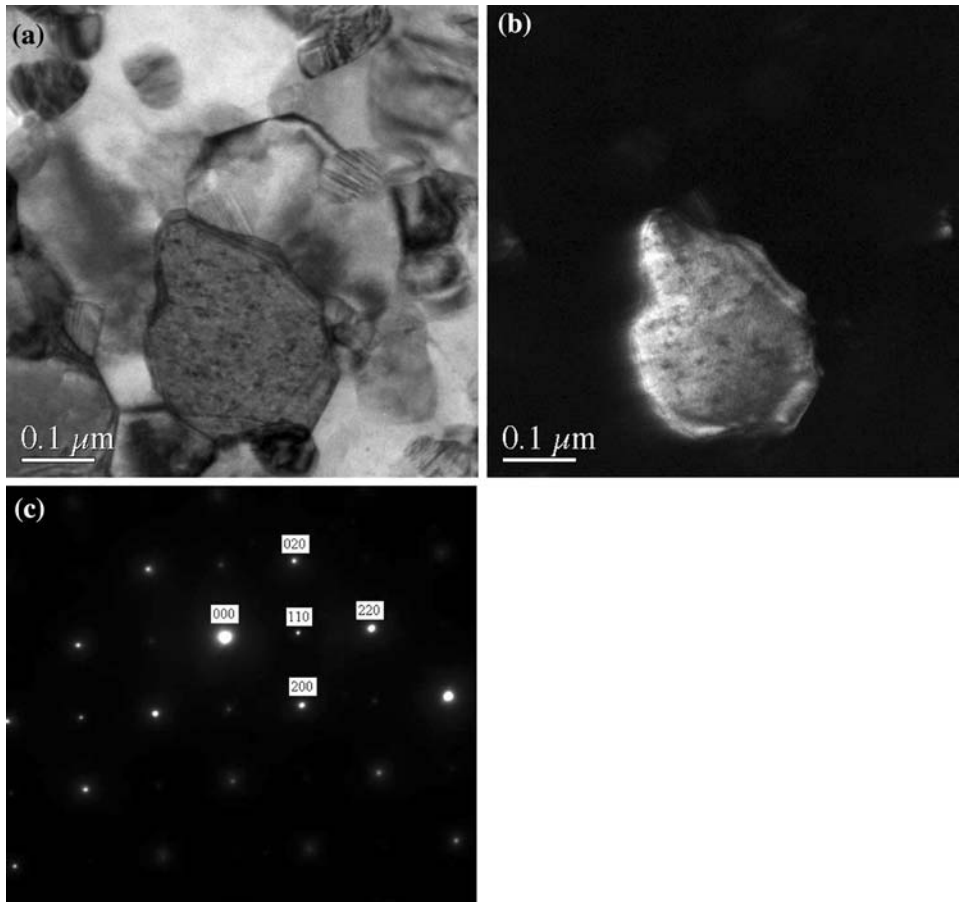

Fig. 10 TEM micrograph of the precipitate from the Fe–Si–Cu–B alloy annealed at 640°C for 1 h: (**a**) bright field image (**b**) dark field image (**c**) SADP: zone axis: [$00\bar{1}$]

Magnetic properties

Cu alloying addition not only had a large effect on the crystallization temperatures, activation energy of crystallization and microstructural evolution, it also affected the magnetic properties. From Figs. 11 and 12 it was observed that both magnetization and coercivity of the two alloys after crystallization showed similar trends. Cu alloying addition decreased the saturation magnetization and coercivity after annealing was carried out after 500 °C for 1 h.

After the alloys were heat-treated at 420 °C for 1 h, crystallization occurred in the Fe–Si–B–Cu alloy, however, the Fe–Si–B alloy remains amorphous, structural relaxation did occur. Due to the formation of Fe_3Si which is a soft magnetic phase, the saturation magnetization of the Fe–Si–B–Cu alloy is higher than that of the Fe–Si–B alloy,

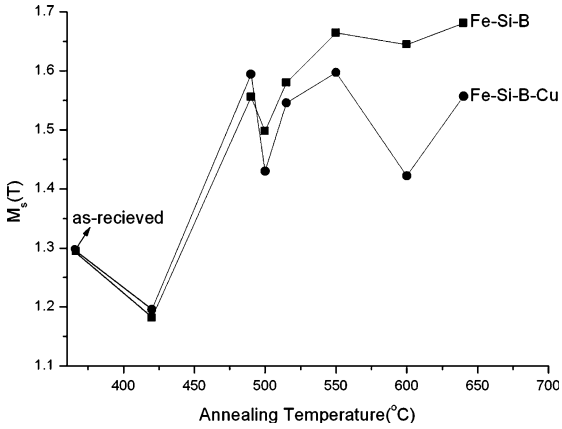

Fig. 11 Magnetization dependence on annealing temperature for annealing time of 1 h

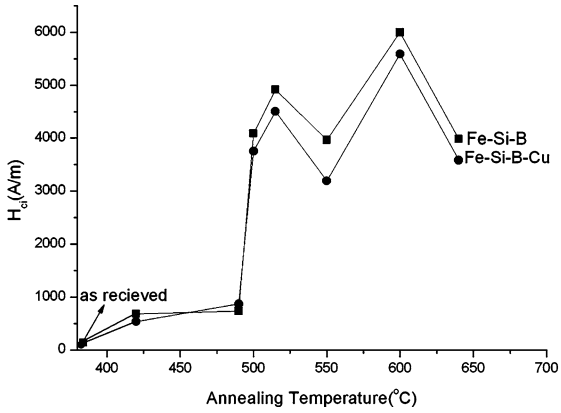

Fig. 12 Coercivity dependence on annealing temperature for annealing time of 1 h

structural relaxation may have caused a lower value of saturation magnetization. The decrease of saturation magnetization may be also in part be attributed to the stresses developed in the amorphous matrix by the growing crystallites which can act as pinning centers for the domain walls. The growing crystallites are far apart from each other so that inter-grain exchange coupling cannot take place, thus the anisotropy cannot be reduced [22].

As the annealing temperature was increased to 490 °C, Cu alloying addition increased the saturation magnetization due to the greater volume fraction of Fe_3Si phase (Fig. 11). The volume fraction of Fe_3Si phase in the Fe–Si–B–Cu alloy is higher than that of the Fe–Si–B–Cu alloy resulting in higher saturation magnetization in the Fe–Si–B–Cu alloy.

As the annealing temperature was increased from 490 °C to 500 °C, a sharp increase of coercivity was observed for both alloys. For the Fe–Si–B alloy the growth of the dendrite increased the coercivity by providing additional obstacles to the motion of the domain walls. For the Fe–Si–B–Cu alloy the formation of the hard magnetic phase Fe_3B at 500 °C caused deterioration of the soft magnetic properties.

However after secondary crystallization began at 500 °C the saturation magnetization and coercivity were decreased in the Cu-containing alloy due to the formation of the Fe_3B phase. Formation of the Fe_3B phase leads to an increase of magnetocrystalline anisotropy, as a result of which magnetic hardening takes place [22]. The coercivity was decreased by Cu alloying addition due to the shape anisotropy in magnetism. At 500 °C the phase formed for the Fe–Si–B alloy as well as the Fe–Si–B–Cu alloy were the same: Fe_3Si phase, however, the morphology showed significant differences. In the case of the Fe–Si–B alloy a dendritic morphology was observed while with Cu alloying addition a spheroidal morphology with rough interfaces was observed. From shape anisotropy considerations the coercivity of the spheroidal morphology can be higher than that of the dendritic morphology [23], thus the coercivity is higher in the Fe–Si–B alloy compared with that of the Fe–Si–B–Cu alloy.

At 550 °C the saturation magnetization again increased due to Fe_3Si phase formation resulting in a higher magnetization value and a lower coercivity value. When the heat treatment is conducted at 600 °C the magnetization decreased less than 0.02 T for the Fe–Si–B alloy while it decreased more than 0.2 T in the case of the Fe–Si–B–Cu alloy due to the decomposition of the Fe_3B phase into Fe–Si and Fe_2B phases, thus the Fe_2B phase lowered the saturation magnetization [24].

Conclusions

A study of the effect of Cu alloying additions on the crystallization behavior of a Fe–Si–B–Cu alloy was conducted by XRD, DSC, TEM and VSM techniques. The following conclusions can be reached:

1. For the Fe–Si–B alloy the primary and secondary crystallization temperatures are 527 and 552 °C, respectively at a heating rate of 10 K/min. With Cu alloying addition the primary and secondary crystallization temperatures were reduced to 466 and 531 °C for the same heating rate.
2. The activation energy of crystallization for the Fe–Si–B alloy was calculated to be 376 kJ/mol for primary crystallization and 342 kJ/mol for secondary crystallization respectively, while that of the Fe–Si–B–Cu alloy is much lower value: 236 and 269 kJ/mol.
3. The phases formed after primary crystallization are the same for both alloys: Fe_3Si. However, the microstructural evolution is significantly different. For the

Fe–Si–B alloy a dendritic morphology is observed after primary crystallization while spheroidal crystals about 100 nm in size were observed after primary crystallization for the Fe–Si–B–Cu alloy.

4. The phases formed after secondary crystallization are the same for both alloys: Fe_3Si, Fe_2B and Fe_3B. The Fe_3Si phase formed in the Fe–Si–B during secondary crystallization was found to have a bcc structure while in the Fe–Si–B–Cu alloy it was found to have a DO_3 ordered structure.
5. Cu alloying addition increased the saturation magnetization during primary crystallization and decreased the saturation magnetization during secondary crystallization. The saturation magnetization and coercivity showed similar trends in both alloys, the extent of the change for the Fe–Si–B–Cu alloy in profile is higher than that of the Fe–Si–B alloy.

Acknowledgement The ribbons used in this study were kindly supplied by Dr. Y. Yoshizawa of Hitachi Metals, Japan.

References

1. Yoshizawa Y, Oguma S, Yamauchi K (1988) J Appl Phys 64:6044
2. Herzer G (1990) IEEE Trans Magn 26:1397
3. Hono K, Hiraga K, Wang Q, Inoue A, Sakurai T (1992) Acta Metal Mater 40:2137
4. Hono K (1999) Acta Mater 47:3127
5. Hono K, Ping DH, Ohnuma M, Onodera H (1999) Acta Mater 47:997
6. Ayers JD, Harris VG, Sprague JA, Elam WT, Jones HN (1997) Nano Mater 9:391
7. Ayers JD, Harris VG, Sprague JA, Elam WT, Jones HN (1998) Acta Mater 46:1861
8. Kulik T (2001) J Non-Crystal Solids 287:145
9. Efthimiadis KG, Polychroniadis EK, Chadjivasiliou SC, Tsoukalas IA (1997) J Magn Magn Mater 171:141
10. Kulik T (1992) Mater Sci Eng A 159:95
11. Noh TH, Lee MB, Jim HJ, Kang IK (1990) J Appl Phys 67:5568
12. Kim WT, Jang PW (1994) Mater Sci Eng A179/A180:309
13. Matko I, Duhaj P, Svec P, Janickovic D (1994) Mater Sci Eng A179/A180:557
14. Zhou F, He KY, Sui ML (1994) Mater Sci Eng A181/A182:1419
15. Marin P, Vazquez M, Olofinjana AO, Davies HA (1998) Nano Mater 10:99
16. Ozawa T. (1970) J Therm Anal 2:301
17. Ping DH, Hono K, Kanekiyo H, Hirosawa S (1999) Acta Mater 47:4641
18. Efthimiadis KG, Polychroniadis EK, Chadjivasiliou SC, Tsoukalas IA (2000) Mater Res Bull 35:937
19. Porter DA, Easterling KE (1992) In: Phase transformation in metals and alloys. Chapman and Hall, London, p. 216
20. Blazquez JS, Franco V, Conde A (2002) J Phys Condens Matter 14:11717
21. Blazquez JS, Franco V, Conde A (2003) Appl Phys A 76:571
22. Hakim MA, Hoque SM (2004) J Magn Magn Mater 284:395
23. Schwarz RB, Shen TD, Harms U, Lillo T (2004) J Magn Magn Mater 283:223
24. Chau N, Hoa NQ, Luong NH (2005) J Magn Magn Mater 290–291:1547